Program Digest, 2019 IEEE International Ultrasonics Symposium (IUS)
Glasgow, Scotland, October 6-9, 2019

Experimental determination of $Al_{1-x}Sc_xN$ thin film thermo-electro-acoustic properties up to 140°C by using SAW resonators

Anli Ding
Technology Department
Fraunhofer Institute for Applied Solid State Physics IAF
Freiburg, Germany
anli.ding@iaf.fraunhofer.de

Nicolas Kurz
Department of Sustainable Systems Engineering INATECH
University of Freiburg
Freiburg, Germany
nicolas.kurz@iaf-extern.fraunhofer.de

Rachid Driad
Technology Department
Fraunhofer Institute for Applied Solid State Physics IAF
Freiburg, Germany
rachid.driad@iaf.fraunhofer.de

Yuan Lu
Epitaxy Department
Fraunhofer Institute for Applied Solid State Physics IAF
Freiburg, Germany
yuan.lu@iaf.fraunhofer.de

Roger Lozar
Microelectronics Department
Fraunhofer Institute for Applied Solid State Physics IAF
Freiburg, Germany
roger.lozar@iaf.fraunhofer.de

Tim Christoph
Technology Department
Fraunhofer Institute for Applied Solid State Physics IAF
Freiburg, Germany
tim.christoph@iaf.fraunhofer.de

Lutz Kirste
Epitaxy Department
Fraunhofer Institute for Applied Solid State Physics IAF
Freiburg, Germany
lutz.kirste@iaf.fraunhofer.de

Oliver Ambacher[1,2]
[1]*Fraunhofer Institute for Applied Solid State Physics IAF*
[2]*Department of Sustainable Systems Engineering INATECH*
[2]*University of Freiburg*
Freiburg, Germany
oliver.ambacher@inatech.uni-freiburg.de

Agnė Žukauskaitė
Epitaxy Department
Fraunhofer Institute for Applied Solid State Physics IAF
Freiburg, Germany
agne.zukauskaite@iaf.fraunhofer.de

***Abstract*—1 µm thick sputtered $Al_{1-x}Sc_xN$ films were used to fabricate SAW resonators with 2-20 µm wavelength and the frequency response was measured in the range of 20 °C to 140 °C. Extracted phase velocity dispersion curve was in good agreement with the simulated dispersion curve by FEM model. Moreover, for each investigated temperature, the corresponding phase velocity shift dispersion curves as a function of normalized thickness were shown in detail for each resonator layer (Si substrate, AlScN piezoelectric layer, and Pt electrode), and the independent thermal influence of the Si, AlScN, and Pt were evaluated. The temperature coefficients of frequency (TCF) of $Al_{1-x}Sc_xN$ (x = 0, 0.14, 0.32) layer was calculated independently and compared with the combined TCFs of the resonators.**

Keywords—AlN, AlScN, SAW Resonator, TCF, FEM

I. INTRODUCTION

Among the available piezoelectric materials, aluminum nitride (AlN) has been widely used in current mobile communication application [1]–[3]. Introducing scandium (Sc) into AlN to form aluminum scandium nitride ($Al_{1-x}Sc_xN$ with up to x≈0.43) can lead to four-fold increase in the piezoelectric coefficient [4] and three-fold increase in the electromechanical coupling coefficient [5], which leads to AlScN being a very promising piezo-acoustic material for next generation mobile communications.

Surface acoustic wave (SAW) devices are key components in telecommunication systems [6] and physical/chemical sensing systems [7], especially when targeting operation in harsh environmental condition [8], [9]. For design and simulation of AlScN-based SAW resonators, the electro-acoustic properties [10] have to be thoroughly investigated. Moreover, as mobile devices' internal temperatures could reach up to 90°C [11], [12] , the temperature dependence of the mentioned properties becomes important. While several reports on thermal characteristics of AlScN-based SAW resonator have been published [13]–[17], obtaining $Al_{1-x}Sc_xN$ temperature coefficients of elasticity which would allow to predict how material coefficients change with temperature remains a challenge. Moreover, future SAW devices will consist of complex layer structure [18], [19], hence it is important to investigate how each layer's behavior contributes to the overall performance of the devices at elevated temperatures. However, such investigation have not been performed until now.

In this work, the theoretical independent thermal influence of the substrate and interdigitated transducer (IDT) materials (Si and Pt, respectively) towards the performance of the $Al_{0.68}Sc_{0.32}N$-based SAW resonators was simulated in 20-140 °C range. Then, resonators were fabricated and their thermo-electro-acoustic performance was evaluated. Based on

the theoretical predictions and the experimental results, the influence of different components of the SAW resonator could be decoupled, enabling us to obtain the thermal influence of $Al_{0.68}Sc_{0.32}N$ material itself. As a result, TCF of $Al_{0.68}Sc_{0.32}N$ was calculated to be -16.41 ppm/K and previously obtained TCF for AlN and $Al_{0.86}Sc_{0.14}N$ based SAW resonators [20] were used to extract the TCF of the piezoelectric layer without the influence of the substrate and the IDT using the same approach. The results obtained here will contribute to the further extraction of much sought for thermal elastic and piezoelectric material parameters of AlScN in the future.

II. Experimental

1 µm thick $Al_{1-x}Sc_xN$ (0001) thin films (x = 0, 0.14 and 0.32) were sputtered on 100 mm diameter high resistivity (>>3.6 kΩ cm) Si(001) substrates using reactive pulsed-DC magnetron co-sputtering from 99.995 % pure Al and 99.99 % pure Sc targets (Evatec Radiance sputter cluster tool, base pressure < $5{\cdot}10^{-6}$ Pa). To remove the native oxide and improve nucleation of the grown layer the substrates were cleaned in-situ for 1 min by a pure argon (Ar) inductively coupled plasma (ICP) etching prior to thin film deposition [21], The total combined magnetron power on Al and Sc targets (P_{Al}+P_{Sc}) was kept constant at 1000W. More details about deposition parameters, growth process optimization, and deposited AlScN film structural characterization can be found elsewhere [22], [23].

Then SAW resonators with wavelengths λ = 2, 2.5, 3, 4, 5, 10, 12, 14, 16, and 20 µm were fabricated. The metallization ratio was kept constant at 50%. Electron beam (e-beam) evaporation together with stepper photolithography/lift-off processes were employed to transfer 100 nm thick platinum (Pt) patterns of the IDT and the reflectors onto the thin films. The IDTs consisted of 50 finger pairs, and each reflector bank at both sides had 40 short-circuited fingers. More details on the device fabrication and characterization can be found elsewhere [20].

The frequency response at every 20 °C from 20°C up to 140 °C and then back to 20°C was measured using Agilent E8361C vector network analyzer (VNA), Cascade Microtech Summit 12151B-S semi-automatic probe station and Temptronic TP03215A thermal chuck in ambient atmospheric conditions. The resonators were allowed to stabilize for 5 minutes at each heating and cooling step before starting the measurements to avoid the drift. Cascade Air Coplanar SG probes (350 µm pitch) were used for all measurements. Calibration was performed on an impedance standard substrate (ISS) from Cascade Microtech using the open-short-load configuration prior measuring.

The modified Butterworth-Van Dyke (mBVD) model [24] was used to fit the measured frequency response of the resonators. The series and parallel resonance frequencies f_s and f_p, respectively, were then calculated from the mBVD parameters:

$$f_s = \frac{1}{2\pi\sqrt{L_m C_m}}, \quad (1)$$

$$f_p = \frac{1}{2\pi}\sqrt{\frac{C_m + C_n}{C_m L_m C_n}}, \quad (2)$$

where L_m, C_m, and C_n are the motional inductance, motional capacitance, and static capacitance, respectively [24].

The relationship between frequency f_s and the resonator wavelength λ was used to calculate the SAW phase velocity v_{ph} [25]:

$$v_{ph} = f_s \lambda. \quad (3)$$

The elastic material constants C_{ij} and their temperature coefficients (TCE) Tc_{ij} for Si were taken from literature [26]. The elastic constants at elevated temperatures were calculated using:

$$C_{ij}(T) = C_{ij}(20) \cdot \left(1 + T_{C_{ij}}^{(1)} \cdot (T-20) + T_{C_{ij}}^{(2)} \cdot (T-20)^2\right) \quad (4)$$

Si density ρ at elevated temperatures was calculated based on coefficients of thermal expansion (CTEs) taken from [27]. The Young's modulus E = 127 GPa and Poisson's ratio υ = 0.3457 of Pt were taken from [28]. All material parameters for Si and Pt used in calculations are given in .

By employing the values in Table 1 in COMSOL MEMS module, 2D SAW model was built and the overall resonator f_s and f_p were extracted from frequency domain sweep as well as the independent influence of Si substrate and Pt IDT at each experimental temperature. Additional details about the geometry of the simulation model and approach could be found

Table 1. Material properties used for calculations [26], [27], [28].

	ϱ (kg/m³)	**α(T) (10^{-6}/K)**	**i,j**	**C_{ij} at 20°C (GPa)**	**1st order TCE $T_{C_{ij}}^{(1)}$ (10^{-6}/K)**	**2nd order TCE $T_{C_{ij}}^{(2)}$ (10^{-9}/K)**
Si	3325.89	$-3.0451 + 0.035705 \cdot T - 7.981 \cdot 10^{-5} \cdot T^2 + 9.5783 \cdot 10^{-8} \cdot T^3 - 5.8919 \cdot 10^{-11} \cdot T^4 + 1.4614 \cdot 10^{-14} \cdot T^5$	1,1	165.7	-73.25	-49.26
			1,2	63.97	-91.59	-32.70
			4,4	79.53	-60.14	-51.28
Pt	21450	N/D	υ = 0.3457, E = 127 GPa		-238.5	N/A

in our previously published work [29]. The detailed explanation of the experimental determination of TCF and hysteresis errors can be found elsewhere [20].

III. RESULTS AND DISCUSSION

Rayleigh mode was excited in SAW resonators in the whole investigated temperature range independently if Sc concentration. Phase velocity dispersion curves were extracted [20] for $Al_{1-x}Sc_xN$ with x = 0, 0.14, and 0.32 using eq. (3). The results are shown in Figure 1. The phase velocity is decreasing monotonically as a function of normalized thickness due to the decreasing substrate influence until the SAW becomes fully confined in the piezoelectric layer at h/lambda ≈ 0.2 [20]. In addition, dispersion curves were computed using finite element method (FEM) based on AlScN material parameters in [29] and they are in good agreement with the experimental data, confirming the good performance of the fabricated structures.

The thermal influence of the substrate and the IDT materials towards the phase velocity v_{ph} at 40°C, 60°C, 80°C, 100°C, 120°C, 140°C was calculated by simulated resonance frequency and are shown in Figure 2 and Figure 3 for Si and Pt, respectively, as a function of normalized thickness h_{AlScN}/λ. Here, the piezoelectric layer thickness h is fixed at 1 µm and the SAW wavelength λ is an independent variable defined as the pitch of the IDT. It is known, that the depth to which the SAW wave penetrates depends on its wavelength [29]–[31] . Therefore, the ratio h_{AlScN}/λ shows the fraction of SAW energy inside the piezoelectric layer. As it can be seen in Figure 2, the thermal influence of substrate material is high at low h_{AlScN}/λ, because the SAW mostly propagates inside the substrate. With increasing h_{AlScN}/λ, SAW propagation becomes increasingly confined to the piezoelectric layer and the substrate influence diminishes, as also shown for the room temperature measurements in Figure 1. On the other hand, as it can be seen in Figure 3, with increasing h_{AlScN}/λ the thermal influence of Pt IDT, which is on top of the piezoelectric layer, increases.

Additional, the total relative v_{ph} shift of $Al_{0.68}Sc_{0.32}N$ SAW resonators at 20°C, 40°C, 60°C, 80°C, 100°C, 120°C, 140°C was calculated by using the VNA measured frequency response. Afterwards, the previous mentioned relative theoretical v_{ph} shifts caused by Si and Pt (Figure 2 and 3) were subtracted yielding the relative v_{ph} shift only caused by piezoelectric layer $Al_{0.68}Sc_{0.32}N$ itself, as shown in Figure 4. It can be seen, that at low h_{AlScN}/λ the thermal influence of $Al_{0.68}Sc_{0.32}N$ is minimal and it increases with increasing h_{AlScN}/λ. This is in agreement with the results of theoretical calculations shown in Figure 2 and 3. With higher h_{AlScN}/λ, the fraction of SAW energy inside the $Al_{0.68}Sc_{0.32}N$ increases and higher difference in relative phase velocity shift is observed between the different temperature curves.

By combining the values from Figure 1, 2, 3, and 4, a distribution of influences from different layers in the SAW resonator can be decoupled, and, in the case of 80°C, all contributions are shown in Figure 5 as a function of normalized thickness h_{AlScN}/λ. Here, the total relative v_{ph} shift changes only slightly throughout the whole investigated h_{AlScN}/λ range, this can be attributed to the the transfer of influence from the deeper-located substrate to the at the surface-located $Al_{0.68}Sc_{0.32}N$ thin film and Pt electrodes.

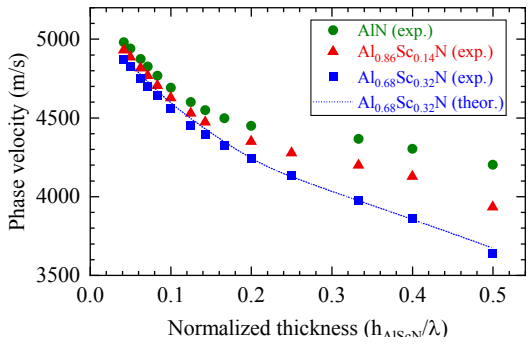

Figure 1. Experimental phase velocity v_{ph} dispersion curves of AlN, $Al_{0.86}Sc_{0.14}N$ and $Al_{0.68}Sc_{0.32}N$-based resonators [20], [29] and the theoretical $Al_{0.68}Sc_{0.32}N$-based resonator dispersion curve computed using extracted material parameters in FEM.

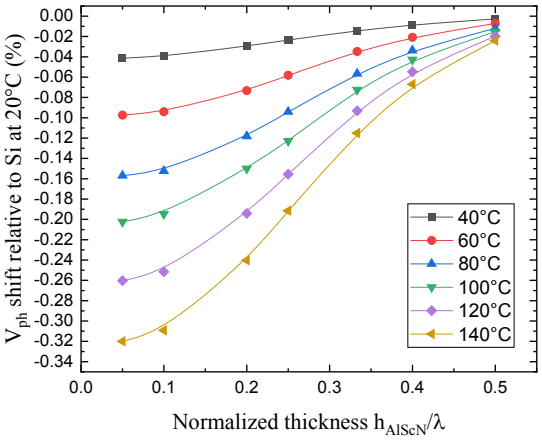

Figure 2. Phase velocity v_{ph} shift dispersion curves at different temperatures relative to 20°C caused solely by thermal change in Si (substrate) material properties as a function of normalized thickness h_{AlScN}/λ.

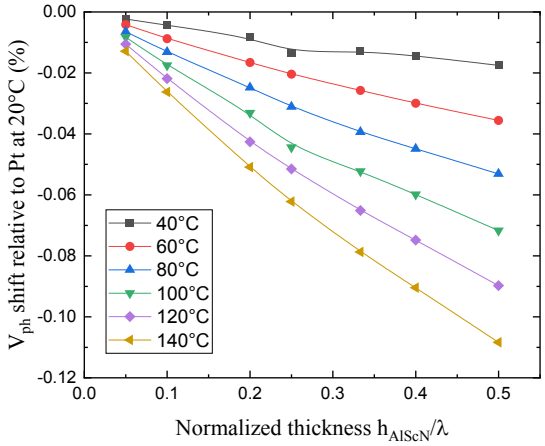

Figure 3. Phase velocity v_{ph} shift dispersion curves at different temperatures relative to 20°C caused solely by thermal change in Pt (IDT) material properties as a function of normalized thickness h_{AlScN}/λ.

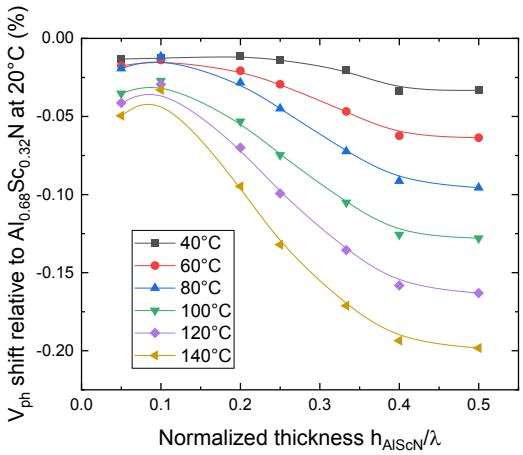

Figure 4. Phase velocity v_{ph} shift dispersion curves at different temperatures relative to 20°C caused solely by thermal change in the $Al_{0.68}Sc_{0.32}N$ (piezoelectric layer) material properties as a function of normalized thickness h_{AlScN}/λ.

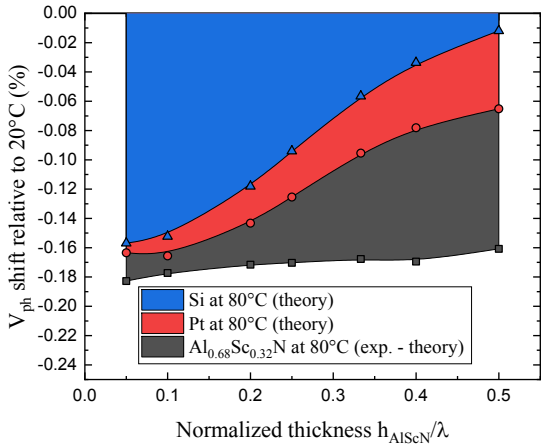

Figure 5. Distribution of the influence of the thermal changes in used materials towards the overall phase velocity v_{ph} shift at 80°C (relative to 20°C) as a function of normalized thickness h_{AlScN}/λ.

Furthermore, the decoupling of individual influences of the materials towards phase velocity enabled to calculate the temperature coefficients of frequency (TCF) of the active piezoelectric layer $Al_{0.68}Sc_{0.32}N$ independently. The TCF for AlN and $Al_{0.86}Sc_{0.14}N$ based SAW resonators were previously published elsewhere [20] and as the influence of the substrate and IDT stays the same for $Al_{1-x}Sc_xN$ SAW resonators regardless of Sc concentration, the corresponding TCF for the AlN and $Al_{0.86}Sc_{0.14}N$ could also be calculated independently. The overview of combined TCFs of the $Al_{1-x}Sc_xN$ based SAW resonator devices and TCFs of the piezoelectric layer alone, i. e. $Al_{1-x}Sc_xN$, are summarized in Table 2.

Table 2. Overview of the temperature coefficients of frequency (TCF) and thermal hysteresis errors δ_{fm} for λ = 2 µm $Al_{1-x}Sc_xN$-based resonators and the TCF of $Al_{0.68}Sc_{0.32}N$ material itself.

	TCF of resonators (ppm/K)[a]	**TCF of $Al_{1-x}Sc_xN$ (ppm/K)**	**δ_{fm} (%)**
AlN	−25.75 ± 0.36 [20]	-15.73	1.07
$Al_{0.86}Sc_{0.14}N$	−25.28 ± 0.13 [20]	-15.22	1.14
$Al_{0.68}Sc_{0.32}N$	−27.49 ± 0.41	-16.41	1.23

[a] Error is given in standard deviation

IV. CONCLUSIONS

Individual thermal influence of the substrate and interdigitated transducer materials (Si and Pt, respectively) towards the performance of the $Al_{0.68}Sc_{0.32}N$-based SAW resonators was calculated at 40°C, 60°C, 80°C, 100°C, 120°C, and 140°C. These theoretical values together with the experimentally obtained phase velocity dispersion curves of the SAW resonators with λ = 2-20 µm fabricated on 1 µm thick sputtered AlScN thin films in the same temperature range were then used to obtain the influence of $Al_{0.68}Sc_{0.32}N$ material itself. Additionally, the independent TCF of $Al_{1-x}Sc_xN$ (x = 0, 0.14, 0.32) piezoelectric layer was calculated and compared with the TCF of the SAW resonator. The results obtained here will improve the understanding of how each layer's behavior contributes to the overall performance of the electroacoustic devices at elevated temperatures. Moreover, the developed methodology can be further used for the extraction of thermal material parameters as TCE as well as strengthen the design and simulation models for future SAW resonator devices with complex layered structures.

ACKNOWLEDGMENT

The authors acknowledge colleagues at Fraunhofer IAF in the Department of Technology for their assistance with the device fabrication and in the Department of Epitaxy for their assistance with the structural analysis characterization. This work was supported by the FhG Internal Programs, under Grant No. Attract 005-600636.

REFERENCES

[1] R. Aigner, "MEMS in RF Filter Applications: Thin-film Bulk Acoustic Wave Technology," *Sensors Updat.*, Vol. 12, Issue 1, Feb. 2003, pp. 175–210.

[2] C. Zhou, Y. Yang, H. Jin, B. Feng, *et al.*, "Surface acoustic wave resonators based on (002)AlN/Pt/diamond/silicon layered structure," *Thin Solid Films*, Vol. 548, Dec. 2013, pp. 425–428.

[3] Y. Zhang, W. Zhu, D. Zhou, Y. Yang, and C. Yang, "Effects of sputtering atmosphere on the properties of c-plane ScAlN thin films prepared on sapphire substrate," *J. Mater. Sci. Mater. Electron.*, Vol. 26, Issue 1, Jan. 2015, pp. 472–478.

[4] M. Akiyama, T. Kamohara, K. Kano, A. Teshigahara, Y. Takeuchi, and N. Kawahara, "Enhancement of piezoelectric response in scandium aluminum nitride alloy thin films prepared by dual reactive cosputtering," *Adv. Mater.*, Vol. 21, Issue 5, 2009, pp. 593–596.

[5] G. Wingqvist, F. Tasnádi, A. Žukauskaitė, J. Birch, H. Arwin, and L. Hultman, "Increased electromechanical coupling in w-$Sc_xAl_{1-x}N$," *Appl. Phys. Lett.*, Vol. 97, Issue 11, 2010, pp. 1–4.

[6] H. Okano, N. Tanaka, Y. Takahashi, T. Tanaka, K. Shibata, and S. Nakano, "Preparation of aluminum nitride thin films by reactive sputtering and their applications to GHz-band surface acoustic wave devices," *Appl. Phys. Lett.*, Vol. 64, Issue 2, 1994, pp. 166–168.

[7] Y. Q. Fu, J. K. Luo, N. T. Nguyen, A. J. Walton, *et al.*, "Advances in piezoelectric thin films for acoustic biosensors, acoustofluidics and lab-on-chip applications," *Progress in Materials Science*, Vol. 89. pp. 31–91, 2017.

[8] G. Macchiarella and G. B. Stracca, "SAW Devices for Telecommunications: Examples and Applications," *Ultrason. Symp. Proc.*, 1982, pp. 247–251.

[9] M. Gillinger, T. Knobloch, M. Schneider, and U. Schmid, "Harsh Environmental Surface Acoustic Wave Temperature Sensor Based on Pure and Scandium doped Aluminum Nitride on Sapphire," *Proceedings*, Vol. 1, Issue 4, Aug. 2017, p. 341.

[10] M. A. Caro, S. Zhang, T. Riekkinen, M. Ylilammi, *et al.*, "Piezoelectric coefficients and spontaneous polarization of ScAlN," *J. Phys. Condens. Matter*, Vol. 27, Issue 24, 2015, p. 245901.

[11] O. Sahin and A. K. Coskun, "Providing sustainable performance in thermally constrained mobile devices," *Proc. 14th ACM/IEEE Symp. Embed. Syst. Real-Time Multimedia, ESTIMedia 2016*, 2016, pp. 72–77.

[12] S.-L. Kuo, C.-W. Pan, P.-Y. Huang, C.-T. Fang, S.-Y. Hsiau, and T.-Y. Chen, "An Innovative Heterogeneous SoC Thermal Model for Smartphone System," in *2018 17th IEEE Intersociety Conference on Thermal and Thermomechanical Phenomena in Electronic Systems (ITherm)*, 2018, Issue 1, pp. 384–391.

[13] W. B. Wang, Y. Q. Fu, J. J. Chen, W. P. Xuan, *et al.*, "AlScN thin film based surface acoustic wave devices with enhanced microfluidic performance," *J. Micromechanics Microengineering*, Vol. 26, Issue 7, Jul. 2016, p. 075006.

[14] M. Gillinger, K. Shaposhnikov, T. Knobloch, M. Schneider, M. Kaltenbacher, and U. Schmid, "Impact of layer and substrate properties on the surface acoustic wave velocity in scandium doped aluminum nitride based SAW devices on sapphire," *Appl. Phys. Lett.*, Vol. 108, Issue 23, Jun. 2016, p. 231601.

[15] F. Bartoli, M. Moutaouekkil, J. Streque, P. Pigeat, *et al.*, "Theoretical and experimental study of ScAlN/Sapphire structure based SAW sensor," in *Proceedings of IEEE Sensors*, 2017, Vol. 2017-Decem, pp. 1–3.

[16] K. Hashimoto, T. Fujii, S. Sato, T. Omori, *et al.*, "High Q surface acoustic wave resonators in 1 to 3 GHz range using ScAlN/single crystalline diamond structure," in *2012 IEEE International Ultrasonics Symposium*, 2012, pp. 1–4.

[17] K. Hashimoto, S. Sato, A. Teshigahara, T. Nakamura, and K. Kano, "High-performance surface acoustic wave resonators in the 1 to 3 GHz range using a ScAlN/6H-SiC structure," *IEEE Trans. Ultrason. Ferroelectr. Freq. Control*, Vol. 60, Issue 3, Mar. 2013, pp. 637–642.

[18] S. Koji Tanaka and T. Norio Nakajima, "Duplexer comprising a SAW filter disposed on a multi-layer substrate," *Geothermics*, Vol. 14, Issue 4, 1985, pp. 595–599.

[19] J. T. Glass, B. A. Fox, D. L. Dreifus, and B. R. Stoner, "Diamond for electronics: Future prospects of diamond SAW devices," *MRS Bull.*, Vol. 23, Issue 9, 1998, pp. 49–55.

[20] A. Ding, M. Reusch, Y. Lu, N. Kurz, *et al.*, "Investigation of Temperature Characteristics and Substrate Influence on AlScN-Based SAW Resonators," *IEEE Int. Ultrason. Symp. IUS*, 2018, pp. 5–10.

[21] M. Schneider, A. Bittner, F. Patocka, M. Stöger-Pollach, E. Halwax, and U. Schmid, "Impact of the surface-near silicon substrate properties on the microstructure of sputter-deposited AlN thin films," *Appl. Phys. Lett.*, Vol. 101, Issue 22, 2012, pp. 1–5.

[22] Y. Lu, M. Reusch, N. Kurz, A. Ding, *et al.*, "Elastic modulus and coefficient of thermal expansion of piezoelectric $Al_{1-x}Sc_xN$ (up to x = 0.41) thin films," *APL Mater.*, Vol. 6, Issue 7, 2018, pp. 0–6.

[23] Y. Lu, M. Reusch, N. Kurz, A. Ding, *et al.*, "Surface Morphology and Microstructure of Pulsed DC Magnetron Sputtered Piezoelectric AlN and AlScN Thin Films," *Phys. Status Solidi Appl. Mater. Sci.*, Vol. 215, Issue 9, 2018, pp. 1–6.

[24] J. D. Larson, P. D. Bradley, S. Wartenberg, and R. C. Ruby, "Modified Butterworth-Van Dyke circuit for FBAR resonators and automated measurement system," *Proc. IEEE Ultrason. Symp.*, Vol. 1, 2000, pp. 863–868.

[25] G. Tang, T. Han, K.-Y. Hashimoto, A. Teshigahara, and T. Iwaki, "Enhancement of effective electromechanical coupling factor by mass loading in layered surface acoustic wave device structures," *Jpn. J. Appl. Phys.*, Vol. 55, Issue 7, 2016, pp. 3–6.

[26] C. Bourgeois, J. Hermann, N. Blanc, N. F. de Rooij, and F. Rudolf, "Determination of the elastic temperature coefficients of monocrystalline silicon," in *International Conference on Solid-State Sensors and Actuators, and Eurosensors IX, Proceedings*, 1995, Vol. 2, pp. 92–95.

[27] H. Watanabe, N. Yamada, and M. Okaji, "Linear Thermal Expansion Coefficient of Silicon from 293 to 1000 K," *Int. J. Thermophys.*, Vol. 25, Issue 1, Jan. 2004, pp. 221–236.

[28] J. Merker, D. Lupton, M. Töpfer, and H. Knake, "High temperature mechanical properties of the platinum group metals: Elastic properties of platinum, rhodium and iridium and their alloys at high temperatures," *Platinum Metals Review*, Vol. 45, Issue 2. pp. 74–82, 2001.

[29] N. Kurz, A. Ding, D. F. Urban, Y. Lu, *et al.*, "Experimental determination of the electro-acoustic properties of thin film AlScN using surface acoustic wave resonators," *J. Appl. Phys.*, Vol. 126, Issue 7, Aug. 2019, p. 075106.

[30] A. A. Oliner, "Acoustic Surface Waves," *Opt. Laser Technol.*, Vol. 9, Issue 5, Oct. 1978, p. 247.

[31] B. A. Auld and R. E. Green, "Acoustic Fields and Waves in Solids: Two Volumes," *Phys. Today*, Vol. 27, Issue 10, Oct. 1974, pp. 63–64.